In Situ Investigation of Si-TPA-MFI Crystallization Using (Ultra-) Small- and Wide-Angle X-ray Scattering

Peter-Paul E. A. de Moor,*,† Theo P. M. Beelen,† Bernd U. Komanschek,‡ Olivier Diat,§ and Rutger A. van Santen†

Schuit Institute of Catalysis, Eindhoven University of Technology, P.O. Box 513, 5600 MB Eindhoven, The Netherlands, Daresbury Laboratory, Warrington WA4 4AD, United Kingdom, and European Synchrotron Radiation Facility, Grenoble, BP 220, 38043, France

Received: July 29, 1997; In Final Form: October 17, 1997[⊗]

The formation of precursors and the growth and aggregation of silicalite-1 crystals using tetrapropylammonium as a template (Si-TPA-MFI) has been studied in situ using X-ray scattering techniques. Simultaneous small-angle and wide-angle X-ray scattering (respectively SAXS and WAXS) experiments using synchrotron light showed that the formation of amorphous colloidal aggregates in water clear synthesis mixtures was dependent on the alkalinity of the solutions. In situ time-resolved ultra-small-angle X-ray scattering (USAXS) showed the form factor oscillations of the growing crystals. Fitting of the USAXS patterns to the scattering pattern of spherical particles having a normal particle size distribution showed a linear growth of the average crystal diameter, which was approximately the same for both alkalinities studied. The final size of the crystals was highest for the synthesis mixture having the highest alkalinity, which can be explained in terms of number of viable nuclei formed. At the end of the linear growth the crystals form aggregates corresponding with a diffusion limited aggregation process (mass fractal dimension of 1.8).

Introduction

Zeolites are crystalline microporous aluminosilicates which are widely used in catalysis, ion exchange, and gas separation processes.[1] Almost all applications require properties of the zeolites which are not met in natural species, and therefore the vast majority of the zeolites used are manmade. Although zeolites can be prepared from nonaqueous synthesis mixtures,[2] they are almost exclusively crystallized under hydrothermal conditions.[3] Improvements of the zeolites presently used and (possible) new applications often require a change in the properties of known zeolites and even new crystal topologies. Therefore many efforts are being made to broaden and deepen the knowledge on reaction processes of the synthesis of zeolites with the main aim to describe rules for the rational design of their synthesis.[4]

In the preparation of high-silica zeolites it is very important to understand the role of the organic structure directing agents.[5−7] One of the key properties of an organic species is to direct the synthesis towards a certain microporous crystalline structure. In water solutions these organic molecules are hydrated, but the hydration is strongly depending on hydrophobic or hydrophilic properties. Successful structure directing agents in zeolite synthesis are believed to have a hydrophobic hydration sphere.[8] The release of this "ordered" water can provide a thermodynamic driving force for the assembly process, when it elicits interactions with hydrophobically hydrated silicates.[9,10]

Apart from information on a molecular scale an understanding about processes on larger length scales is indispensable, e.g., for the detection of long range order and to study the formation and transformations of an amorphous gel phase. While the presence of long range order can easily be tested by ex situ X-ray diffraction, the characterisation of the amorphous gel is more difficult because the length scale to be probed does not allow the use of spectroscopic techniques. Additionally the structures to be investigated are very fragile, and therefore only in situ techniques can give reliable results. We demonstrated earlier that in situ time resolved combined small- and wide-angle X-ray scattering can give valuable information on both the long range order and the formation of amorphous colloidal structures.[11] For the synthesis of Si-TPA-MFI from a clear solution we found the formation of amorphous colloidal aggregates (size ∼ 7 nm) prior to the onset of crystallization. As soon as the first signs of MFI-Bragg reflections appeared in the WAXS pattern, changes in the SAXS pattern showed the formation of particles larger than 50 nm. Since these patterns corresponded with the formation of mass fractal aggregates,[12] a provisional crystallization mechanism was described involving a second aggregation step with the colloidal aggregates as primary particles. Recently we demonstrated[13] that the formation of colloidal aggregates depends on the alkalinity of the synthesis mixture and that the crystallization of Si-TPA-MFI is also possible without their presence at any stage during the reaction. However, the *d*-values needed to be probed to obtain information on the second aggregation step as well as information about the growing crystals could not be obtained in previous studies.

To extend in situ experiments to length scales between 50 nm and several micrometers, scattering with larger wavelengths can be applied, for example, scattering with visible light.[14,15] A disadvantage of visible light scattering for our system is that it cannot be used for turbid samples, and, in the case of an aggregating system, the size of the individual particles cannot be determined. Therefore it can only be used ex situ at advanced stages of the crystallization process by diluting the samples and cannot be used for samples in which a heterogeneous gel phase is formed.

An altenative is to exploit scattering of X-rays at much

* Author of correspondence: fax +31 40 2455054, e-mail ppaul@sg3.chem.tue.nl.
† Eindhoven University of Technology.
‡ Daresbury Laboratory.
§ European Synchrotron Radiation Facility.
⊗ Abstract published in *Advance ACS Abstracts,* December 1, 1997.

S1089-5647(97)02478-4 CCC: $14.00

smaller angles with a Bonse-Hart type of camera. The efficiency of this type of camera is low (crystal analyzer, zero-dimension detection which imposes a 2Θ scan), and therefore high-brilliance synchrotron radiation has to be used and only static experiments can be performed due to the long data acquisition times. Recently a Bonse-Hart camera has been developed[16,17] at the high-brilliance beamline ID2/BL4[18,19] of the European Synchrotron Radiation Facility (ESRF). The high brilliance of the beam allows a USAXS pattern to be obtained every 15 min, which, to our knowledge, is unique in zeolite investigations.

In this study we report on both simultaneous SAXS and WAXS experiments and USAXS experiments on the crystallization of Si-TPA-MFI from clear solutions with synthesis mixtures of different alkalinities. By combining these results, we obtain information on a very broad range of scattering angles providing information about the amorphous precursor phase as well as the crystals formed.

Small-Angle X-ray Scattering

Small-angle scattering of X-rays is observed when electron density inhomogeneities on a colloidal scale exist in the sample.[20] The detected intensity as a function of the scattering angle Θ, described in terms of $Q = (4\cdot\pi/\lambda)\cdot\sin\Theta$, can be written as[21]

$$I(Q) = \phi\cdot P(Q)\cdot S(Q) \tag{1}$$

ϕ is the number density of the particles or the individual scatterers in the sample. The form factor $P(Q)$ describes the relation between the geometry of the individual particles and their scattering. The structure factor $S(Q)$ contains information on the correlation of these particles.

The general mathematical description (using Debye approximation) of the form factor is[22]

$$P(Q) = I_e N_e^2 \frac{\int_0^L g(r)\frac{\sin(Qr)}{Qr} r^2\,\mathrm{d}r}{\int_0^L g(r) r^2\,\mathrm{d}r} \tag{2}$$

where I_e = the scattered intensity per electron, N_e = the number of electrons per scatterer, and $g(r)$ = the electron density correlation function. Using this formula in principle the form factor for all types of particles can be calculated, though only for a limited set of morphologies a solution has been found.[23] The form factor for a homogeneous sphere with electron density ρ and radius R is given by

$$P(Q) = V^2(\rho - \rho_0)^2\left[3\frac{\sin(QR) - QR\cos(QR)}{(QR)^3}\right]^2 \tag{3}$$

Here ρ_0 is the electron density of the medium surrounding the particle and V the volume of the scattering entity. If we have a polydisperse system of homogeneous spheres with a particle size distribution $D(r)$ for which, $\int_0^\infty D(r)\,\mathrm{d}r = 1$, then the scattered intensity in the case of noninteracting particles is given by[24]

$$I(Q) = \phi\int_0^\infty D(r)\cdot P(Q,r)\,\mathrm{d}r \tag{4}$$

Figure 1 shows the calculated intensities for populations of noninteracting particles with different normal number particle size distributions. Upon increasing polydispersity the maxima and minima are less pronounced, and in the log $I\cdot Q^4$ vs log Q plot one observes that their position shifts to smaller angles.

In almost all experiments, the concentration of the scattering entities is such that one has to account for the particle interactions,[25] using the structure factor $S(Q)$. The scattering theory relates $S(Q)$ via a Fourier transform with the pair correlation function $g(r)$, describing the chance to find another particle within a distance r from a certain particle[27]

$$S(Q) = 1 + 4\pi\phi\int_0^\infty |g(r) - 1| r^2 \frac{\sin(Qr)}{Qr}\,\mathrm{d}r \tag{5}$$

In some systems the individual scattering particles form aggregates with mass fractal properties.[27] For such structures the pair correlation function can be related to the mass fractal dimension D_f, and substitution in eq 5 and solving the Fourier transformation leads to the following structure factor[21]

$$S(Q) = 1 + \frac{D_f\Gamma(D_f - 1)}{(Qr_0)^{D_f}\left(1 + \frac{1}{Q^2\xi^2}\right)^{(D_f-1)/2}}\sin|(D_f - 1)tg^{-1}(Q\xi)| \tag{6}$$

Here $\Gamma(x)$ is the Gamma-function, r_0 is the size of the individual particles, and ξ corresponds to the size of the aggregate. In regions where this structure factor dominates the scattering intensity behavior ($r_0 < Q^{-1} < \xi$), one finds $I(Q) \sim Q^{-D_f}$. This mass fractal dimension can give information about the mechanisms controlling the aggregation process and the transformations in the structures formed[27,28] and can have values between 1 and 3.

It has been shown[29,30] that scattering from particles with surface fractal properties results in $I(Q) \sim Q^{-\alpha}$, with $\alpha = 6 - D_s$ (D_s = surface fractal dimension). Because D_s ranges from 2 (smooth) to 3 (extremely rough), α will vary between 3 and 4 (Porod slope of -4 in the log I vs log Q plot).

In practical situations one always has to evaluate the influence of the imperfectness of the experimental setup on the signal measured. In small-angle scattering, three characteristics of the experimental design can give rise to distortion of the scattering curves:[31,32] the collimating system, the detector system, and wavelength effects. The general influence of all three types of distortions on the signal measured is a smearing effect, in which the maxima and minima become less pronounced and the slope of the curve is changed. This problem was already known in the 1950s as well as the solution for the case of an infinite slit (Guinier,[22] pp 111−120). Many papers have been published on proposed correction methods (overviews given by Schmidt[33] and Lambard et al.[34] Early methods used the differentiation of the measured signal, introducing relatively large error. In this work we used an iterative method which does not need differentiation.[35]

Experimental Section

Si-TPA-MFI Synthesis. The recipe used is based on a patent of Exxon Chemical.[36] Synthesis mixtures with a chemical composition xNa$_2$O/1.22(TPA)$_2$O/10SiO$_2$/117H$_2$O, where x = 0.434 (Si/OH = 3.02) or x = 0.848 (Si/OH = 2.42) have been prepared as follows.

1.40 g (for Si/OH = 3.02) or 2.74 g (for Si/OH = 2.42) NaOH (Merck, p.a.) was dissolved in 100 g of tetrapropylammonium hydroxide (Merck, 20 wt % TPAOH in H$_2$O) with gentle mixing at room temperature, followed by spoonwise addition of 27.0 g of silicic acid powder (Baker, 10.2 wt % H$_2$O). Thereafter the homogeneous dispersion was boiled under stirring for approximately 10 min to obtain a clear solution. The solution was cooled down to room temperature in a water bath, corrected for loss of water during boiling, and filtered through a paper

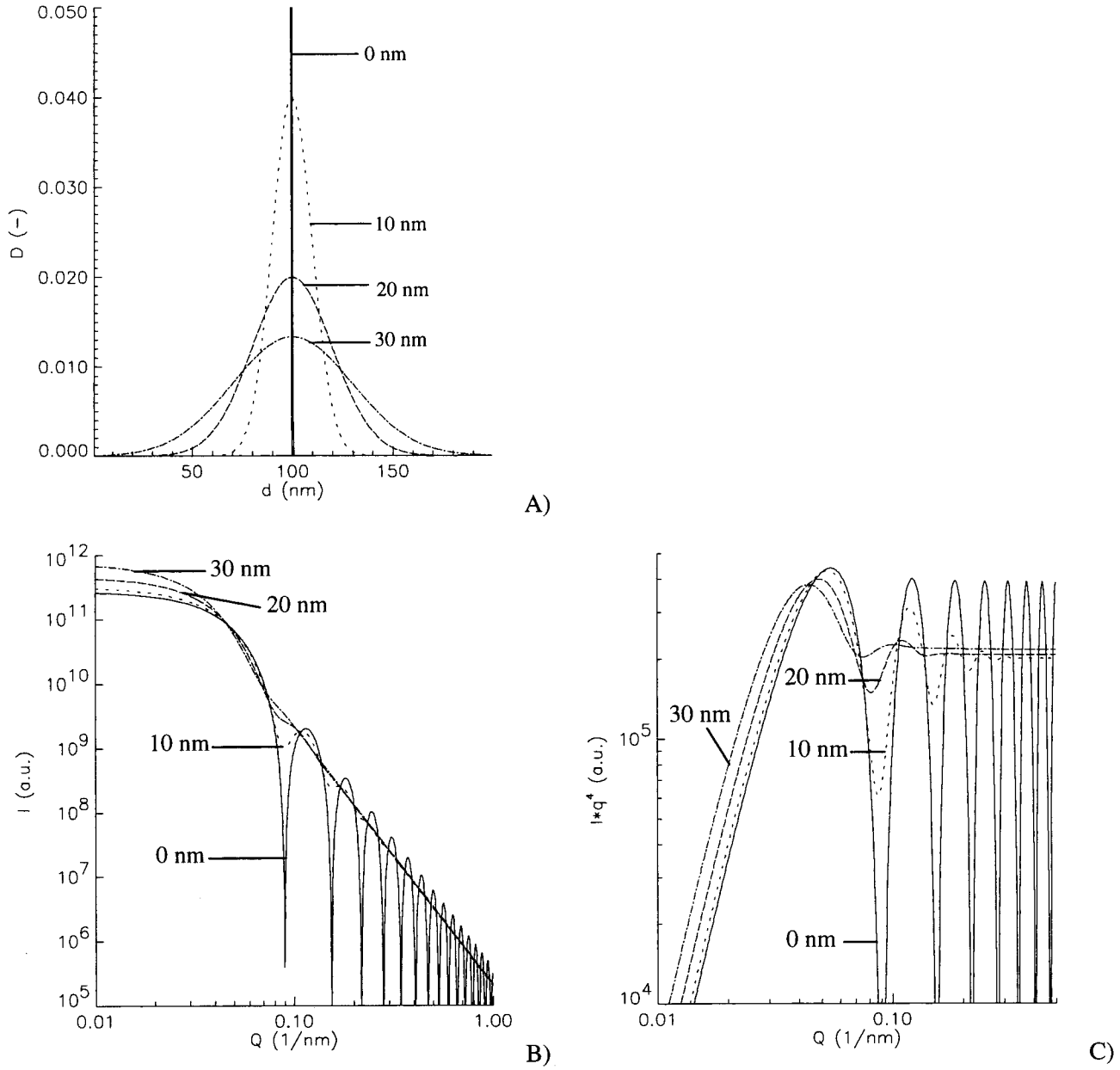

Figure 1. Normal particles size distributions (A) with $\mu = 100$ nm and $\sigma = 0$, 10, 20, and 30 nm (annotated at the curves), the corresponding calculated scattering patterns assuming noninteracting particles (B), and a plot of log $I{\cdot}Q^4$ vs log Q of the same data (C).

filter (Schleicher & Schüll, Schwarzband). The reaction mixtures were completely clear, and aging at room temperature before heating to a reaction temperature of 125 °C was less than 1 h.

To perform in situ experiments, we designed an electrically heated brass holder containing a rotating round sample cell. Rotation was necessary to keep the synthesis mixture homogeneous since only a small spot near the center of the cell is exposed to the X-ray beam. A rate of approximately 2 revolutions per minute appeared to be fast enough to prevent silicalite crystals from precipitating prematurely.

Two clear mica sheets (Attwater & Sons) are used as windows, with spacing provided by a Teflon ring (thickness 0.5 mm). The liquid sample can be heated hydrothermally up to 175 °C, and contact between the sample and the brass cell is avoided at any moment during the sample preparation or the synthesis. Heating of the sample holder from room temperature to a reaction temperature of 125 °C took only 2 min. This rotating cell has been used for both the combined SAXS/WAXS and the USAXS investigation.

SAXS/WAXS. The time-resolved simultaneous SAXS and WAXS experiments were performed at station 8.2 of the Synchrotron Radiation Source (Daresbury Laboratory, Warrington, U.K.). The length of the vacuum chamber between the sample and the SAXS detector was 3.3 m, and the resulting ranges covered with the detectors are reported in Table 1. The SAXS data were recorded using a position sensitive multiwire gas-filled quadrant detector. The WAXS patterns were collected using a position sensitive pressurised gas detector (INEL). The wavelength of the X-rays was 1.54 Å and $\Delta\lambda/\lambda < 4 \times 10^{-3}$. More details concerning the camera geometry, data collection, and detectors are given by Bras et al.[37] and Lewis et al.[38]

The intensity of the scattered X-rays was sufficient to collect a small-angle and wide-angle X-ray scattering pattern with an acceptable signal-to-noise ratio every 2 min. The WAXS pattern were used to determine the crystallization behavior and to check for other crystalline phases than MFI. The integrated intensity in the range between $2\Theta = 22.0°$ and 25.1°, where several strong Bragg reflections of MFI are located is used as a measure for the crystallinity of the sample under investigation. This way

TABLE 1: Ranges Covered in the Experiments

setup, detector	2Θ (deg)	Q (nm^{-1})	d (nm)
SAXS, quadrant	0.18−3.51	0.13−2.5	48−2.5
WAXS, curved-INEL	12−54	8.5−37	0.74−0.17
Bonse-Hart, 1 analyzer cryst., NaI scint.	(1.4×10^{-3})−0.45	0.001−0.32	6300−20
Bonse-Hart, 2 analyzer cryst., photodiode	(1.4×10^{-3})−0.20	0.001−0.14	6300−45

we also take into account possible line broadening due to the formation of relatively small crystallites.

To calibrate the SAXS and WAXS detector, the scattering patterns of respectively an oriented specimen of wet rat tail collagen and a sample of fully crystallized zeolite NaA (Procter & Gamble) have been used. The SAXS data were corrected for the detector sensitivity and X-ray beam intensity prior to background subtraction. The scattering signal of water between two mica windows at 125 °C was used as background. The WAXS patterns were corrected for the incident beam decay.

USAXS. A Bonse-Hart type of X-ray camera[16,17] at the high brilliance small-angle scattering station ID2/BL4 at the European Synchrotron Radiation Facility (ESRF)[18,19] has been used to record the ultra-small-angle X-ray scattering data. The data reported here have been recorded during two beam time allocations using different setups. The reproducibility of each setup at different runs is expected to be better than for different setups as reported here.

During our first session we used only one analyzer crystal (Si(220)) with three reflections in the horizontal plane. A second analyzer crystal has been omitted to obtain sufficient intensity. Therefore the data of this session had to be corrected for collimation effects. For the deconvolution procedure we used a program based on the method of Lake[35] and written by Lesieur,[34] which iteratively calculates the deconvoluted scattering pattern using a weighting function accounting for the collimation effects. The intensity distribution of the X-ray beam at the sample position is described by a trapezium, of which the large base and small top were determined to be respectively 0.5 and 0.2 mm. The height of the analyzer slit was 1.0 mm, and the sample to detector distance was 300 mm.

The setup for our second session also had an additional second analyzer crystal (Si(111)) with two reflections in the vertical direction in order to get a final high-resolution detection in the horizontal plane. Therefore no desmearing of the measured patterns was needed, although at the cost of lower scattering intensities and therefore resulting in a lower Q limit with an acceptable signal to noise ratio. Therefore the upper Q limit was lower compared to the first session (see Table 1). As a detector a NaI scintillator or a photodiode were used, which both showed a linear response over an intensity range of 4 decades. Several scans (4−5) over different 2Θ-ranges with sufficient overlap were recorded using different degrees of attenuation of the incident X-ray beam, in order to have intensities on the detector in the linear range. The wavelength of the X-rays used was 0.99 Å with $\Delta\lambda/\lambda = 3 \times 10^{-4}$.

Electron Microscopy. The samples for the electron microscopy (EM) experiments were also prepared in the synthesis cell used for the SAXS/WAXS and USAXS experiments under the same conditions. After rapid cooling of the cell to room temperature after a certain reaction time, the sample was filtered and washed extensively with deionized water over a 0.02 μm filter (Whatman, Anodisk).

Transmission electron microscopy was performed at Delft university using a Philips CM 30 T electron microscope with an LaB_6 filament as the source of electrons operated at 300 kV. Samples were mounted on a carbon polymer supported on a copper grid by rubbing the grid against the filter containing the sample, followed by sputtering with carbon to decrease charging in the microscope.

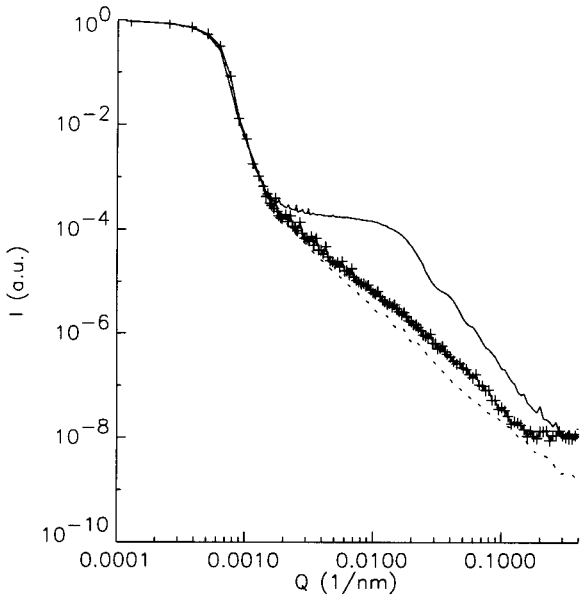

Figure 2. USAXS patterns of the background signal (dotted line), a synthesis mixture before the formation of crystals (plus signs) and after crystallization (solid line). The high-intensity at Q-values lower than 0.001 nm^{-1} correspond to the direct beam.

Results

USAXS Data Treatment. The scans with the Bonse-Hart setup, over different intervals of scattering angles, taken with different degrees of attenuation of the incident beam, have been merged to form one pattern. Figure 2 shows the background pattern together with examples of scattering patterns at a short reaction time and a time when crystals are formed. At reaction times when no crystals have been formed yet, or when the concentration of crystals is very low, the signal is just above the background signal, resulting in low signal to noise ratios. When the crystals have been formed, the intensity is a factor 10 or more higher than the background over a large Q range. The scattering patterns obtained with the Bonse-Hart setup using one analyzer crystal have been desmeared for the X-ray beam shape and the height of the analyzer slit after background subtraction. This desmearing process had a pronounced influence on the slope of the log I vs log Q plot of the scattering patterns (see Figure 3). The decrease in the slope ($-3.2 \rightarrow -4$) corresponds with the decrease observed for the slope in the Porod region of a sphere before and after correction if the X-ray source is an infinite slit ($-3 \rightarrow -4$). It also revealed an intensification of the oscillating pattern which corresponds to the form factor of the scattering crystals, and there was a slight decrease in the signal to noise ratio.

During our second USAXS session we studied the same syntheses also for longer reaction times, this time using two analyzer crystals and therefore omitting the need to desmear the scattering patterns. Figure 4 shows a comparison of the desmeared result of a pattern measured with a setup with one analyzer crystal, with a corresponding one obtained with two analyzer crystals.

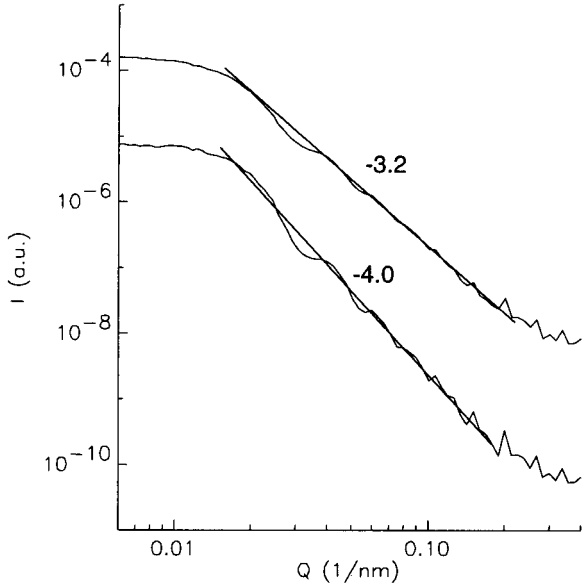

Figure 3. USAXS scattering pattern after crystallization, before (upper curve) and after desmearing (lower curve).

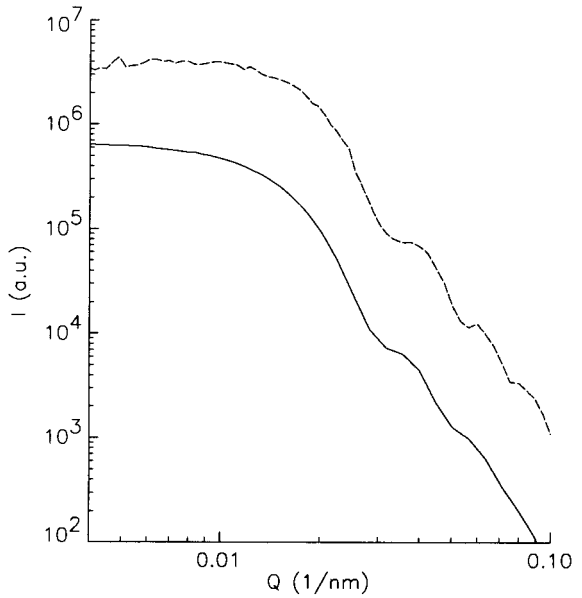

Figure 4. USAXS pattern obtained with a Bonse-Hart set-up with one analyzer crystal (broken line, time = 286 min) and with a setup having two analyzer crystals (solid line, time = 263 min) for the synthesis of Si-TPA-MFI with Si/OH = 2.42.

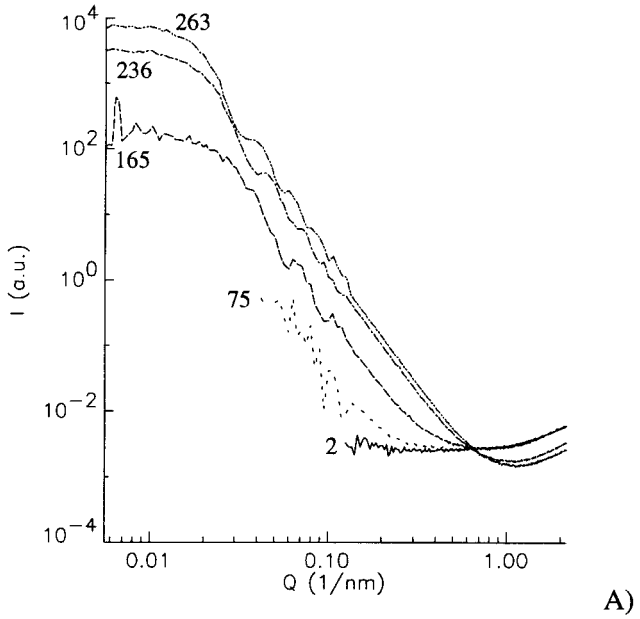

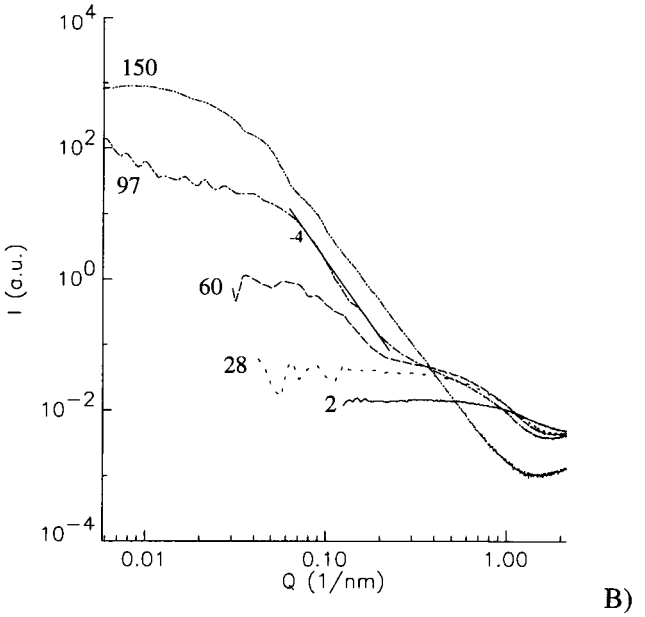

Figure 5. Combined SAXS and USAXS patterns for several reaction times (denoted at the curves in minutes): (A) Si/OH = 2.42 and (B) Si/OH = 3.02. The slope of the linear fit is −4.

SAXS/WAXS. The USAXS data of our first session had a good overlap in *Q*-range with our SAXS-data (Table 1). Figure 5 shows the merged USAXS and SAXS patterns for synthesis mixtures with Si/OH = 3.02 and Si/OH = 2.42 after several reaction times, giving information on a very broad *Q*-range. At relatively short reaction times the signal to noise ratio at low *Q*-values was too low to be plotted.

Figure 6 shows the WAXS patterns for the synthesis with Si/OH = 2.42 as a function of time and provides information on the presence of crystalline phases. Bragg reflections appeared when the reaction time exceeds 100 min. The detected patterns showed that MFI was formed in all syntheses and that no other crystalline phase was present at any time during the reaction; however, the onset of crystallization depended on the Si/OH-ratio.

After ∼30 min of heating to reaction temperature, a distinct difference between the scattering curves for the two synthesis mixtures was observed: The scattering of the system with Si/OH = 3.02 shows the formation of an increased intensity in the *Q*-range between 0.5 and 1.5 nm^{-1} (see Figure 5B), compared to the scattering of the system with Si/OH = 2.42 in this range which did not change between 2 and 50 min of reaction. The intensity at $Q = 0.6$ nm^{-1} as a function of time can be used as a measure for the intensity of this hump and is compared with the crystallization behavior in Figure 7.

Fitting USAXS Patterns. Because the USAXS patterns extend to low *Q*-values, the size of the growing crystals can be determined by fitting calculated patterns corresponding to particles of a certain diameter or particle size distribution to the measured curve (typically for $Q < 0.2$ nm^{-1}). Figure 8 compares the results of fitting an observed USAXS pattern with both a population of noninteracting particles with a single diameter and with a population with a particle size distribution. It is clear that the fit to a size distribution is better than the fit with a single diameter. There are still some systematic differences between the calculated and measured profiles for populations with a size distribution. In all cases the intensity

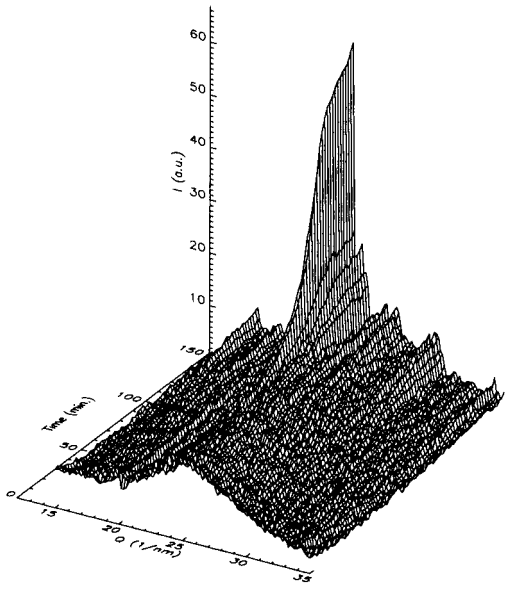

Figure 6. WAXS patterns as a function of time for the crystallization of Si-TPA-MFI from a synthesis mixture having Si/OH = 2.42.

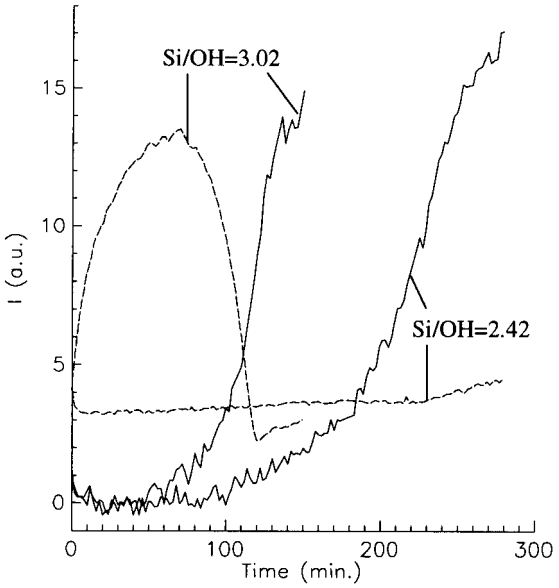

Figure 7. Crystallinity (solid lines) as determined from the WAXS-data as a function of time for both systems, together with the intensity in the SAXS due to scattering at the amorphous colloidal aggregates at $Q = 0.6$ nm^{-1} (broken lines).

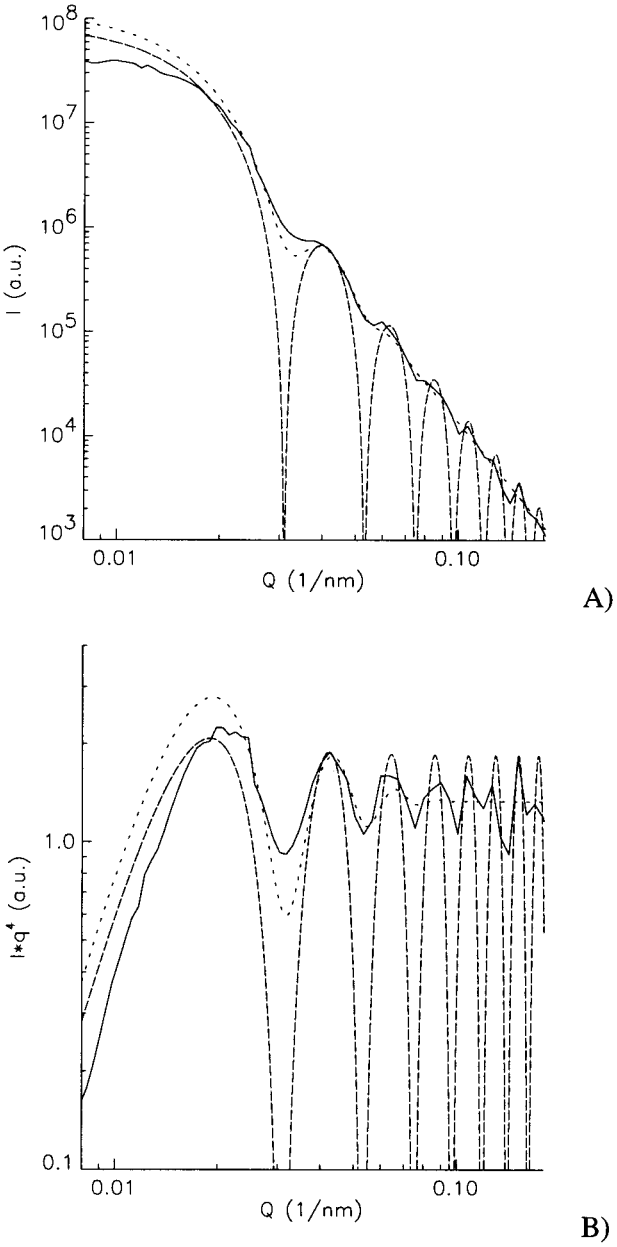

Figure 8. Fitting of the scattering pattern of the system with Si/OH = 2.42 after 263 min of reaction (solid line) with the calculated scattering pattern a population of homogeneous spheres with a normal number particle size distribution with an average of 270 nm and a standard deviation of 35 nm (dotted line), and with the pattern corresponding to a single diameter of 290 nm (broken line). Fitting of the log I vs log Q plot (A) and the log $I{\cdot}Q^4$ vs log Q representation of the same data (B).

of the observed scattering pattern is lower than the calculated one for Q-values below the first maximum in the log $I{\cdot}Q^4$ vs log Q plot. The structure factor effects can only be ignored in very diluted systems,[25,39,40] where the influence of particle interactions on the scattering is negligible. In case of interactions with no tendency to aggregate, a decrease of the observed scattering intensity at angles lower than those corresponding with the size of the scattering entities has to be expected. Due to this influence of the particle interactions on the scattering pattern, it is not correct to determine the average size of the scattering particles from the crossover to the Porod region, nor by the locus of the first maximum in the log $I{\cdot}Q^4$ vs log Q plot (see Figure 8). Therefore, in our fitting procedure we focused on agreement between the location of the minima and maxima at higher Q-values than the first maximum in the log $I{\cdot}Q^4$ vs log Q plot (e.g. concentrated at $Q > 0.025$ nm^{-1} in Figure 8), where the contribution of the structure factor is negligible. Doing so, we found in almost all fitted patterns that the first two maxima in the log $I{\cdot}Q^4$ vs log Q plot, and the minimum between them are more pronounced in the calculated pattern compared to the observed one, suggesting a lower degree of monodispersity than the one used for the calculation. Contrary, at higher Q-values, the form factor oscillations decay faster in the calculated pattern than in the measurement, pointing to a higher degree of monodispersity of the measured system compared to the one used for the calculation.

Possible explanations for this contradiction are the influence of the structure factor, the imperfection of the desmearing method,[17] and the imperfect spherical shape of the crystals. EM-photographs show that the shape of the crystals do not show the typical MFI shape with 90° twinning,[41−43] but the faces are rounded as often seen under conditions favoring fast growth of crystals and in stages that the growth of the crystals is not yet

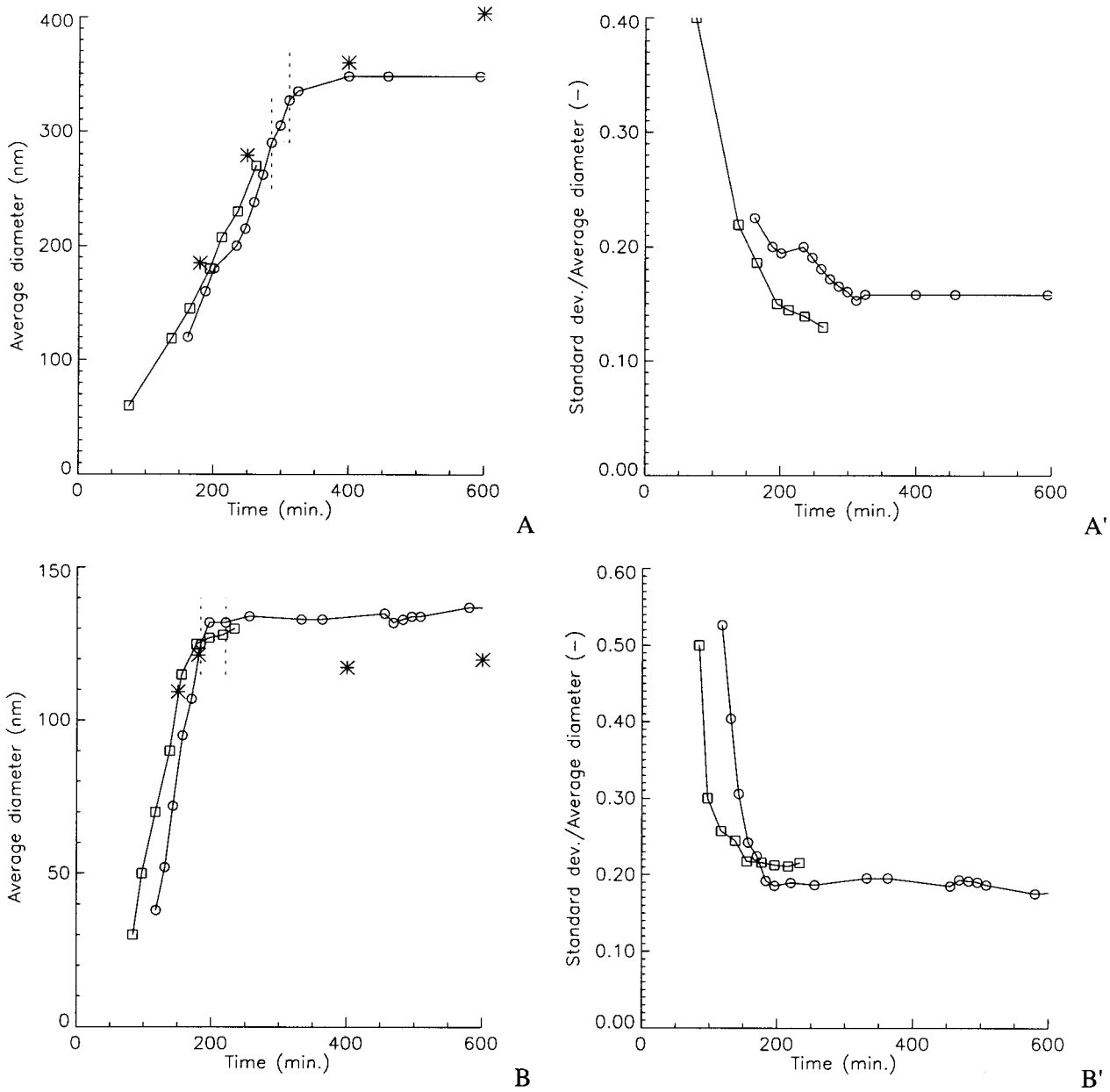

Figure 9. Average diameter and (standard deviation/average diameter) of the particle size distribution of the crystals for syntheses with Si/OH = 2.42 (A) and Si/OH = 3.02 (B). The dotted lines indicate the time ranges in which crystal aggregation was observed. (□) one analyzer crystal, (○) two analyzer crystals. The asterisks denote the average diameter as determined from electron micrographs.

complete. However, we applied the form factor of perfectly spherical particles (eq 3). The use of a model for particles having a lower degree of symmetry will always lead to less pronounced first maxima and minima in the form factor,[23] but for small deviations from spherical particles, the location of the maxima and minima will not be affected much.

The results of the fitted USAXS data are shown in Figure 9. The arithmetic mean diameter of the particles determined by the fit is quite accurate since it is deduced from the sharp positions of minima and maxima in the log $I \cdot Q^4$ vs log Q plot, and correspond very well to the average diameter of the crystals as determined from electron microscopy photographs (Figure 9). For both syntheses and both USAXS-sessions we found a linear growth of the average crystal size with the reaction time: 1.12 and 1.33 nm/min for Si/OH = 2.42, 1.18 and 1.27 nm/min for Si/OH = 3.02. The data concerning the width of the particle size distribution has to be treated with care, since these results are much more sensitive to the possible distortions of the observed pattern than the average diameter. The ratio of the standard deviation and the average of the particle size distribution, being a measure for the polydispersity, is decreasing continuously during crystal growth (Figure 9).

Crystal Aggregation. Using USAXS we also studied the crystallization process for longer reaction times. After 183 (Si/OH = 3.02) and 286 min (Si/OH = 2.42), respectively, we observed a sudden increase in intensity in the low Q-region (see Figure 10). Again this effect is due to particle interactions, but now resulting in an increase in intensity. This agrees with a model in which the individual scattering entities are aggregated to larger structures. The slope of the linear fit in the low Q-region of the log I vs log Q plot is approximately −1.8 and remains constant in time. For the synthesis with Si/OH = 2.42 using one analyzer crystal, this effect was not observed since no data is available at longer reaction times than 265 min.

Discussion

SAXS/WAXS and USAXS Results. The small-angle scattering curves observed after 2 min of heating of the synthesis mixtures showed an almost homogeneous scattering over the

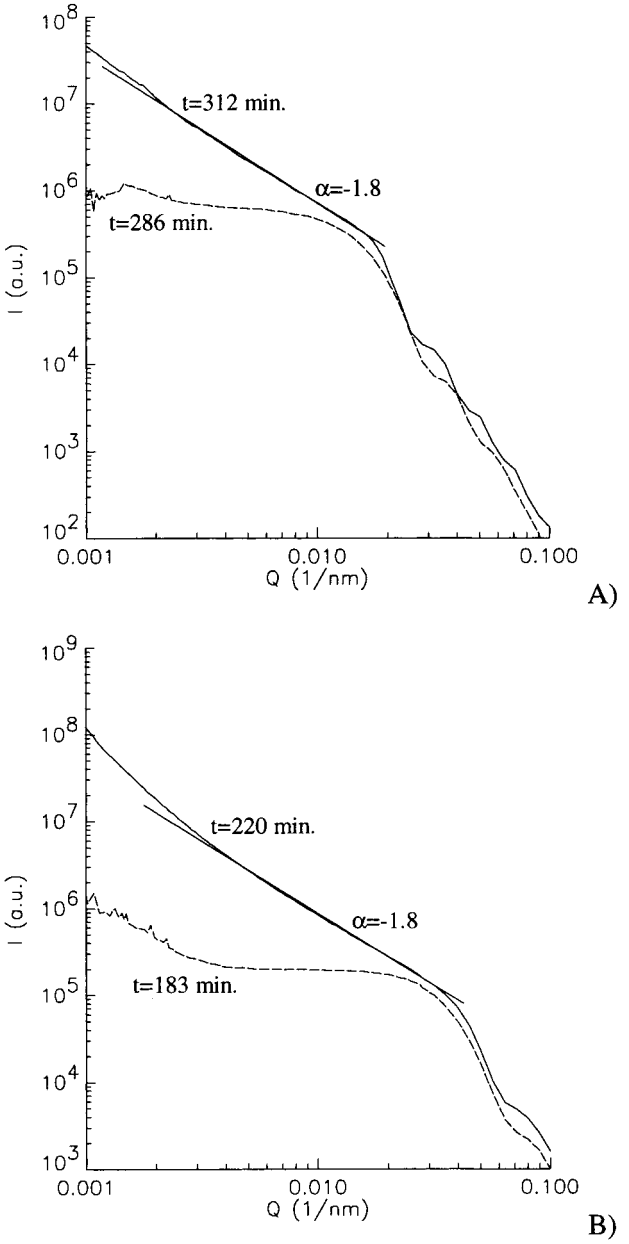

Figure 10. USAXS patterns showing the increase in scattering intensity at very low Q-values due to the aggregation of the crystals for (A) Si/OH = 2.42 and (B) Si/OH = 3.02. The slopes α correspond to the linear fit with $I(Q) \sim Q^{-\alpha}$.

whole available Q-range. Therefore it is believed that the silicic acid was completely dissolved to silica monomers, oligomers, and polymers with a size too small to be observed in the available Q-range.

After several tens of minutes of reaction time, a broad feature in the SAXS pattern appeared at $Q = 0.5-1.5$ nm^{-1} during the synthesis with Si/OH = 3.02, while this hump is absent for the system with Si/OH = 2.42. In an earlier study[11] we interpreted this feature as being due to scattering from amorphous colloidal aggregates with a size of around 7 nm. Later[13] we found the formation of this colloidal aggregate to be dependent on the alkalinity of the synthesis mixture: for Si/OH values higher than 2.65 colloidal aggregates are formed, while they are not observed for lower values. The size of the aggregates was estimated to be around 10 nm. At longer reaction times (≥60 min), the intensity increases at lower angles due to the scattering of colloidal aggregates (Q < 0.3 nm^{-1}). Due to the restricted Q-range available, this was first interpreted[11] as a second aggregation step with the colloidal aggregates present in the solution being the primary particles. Based on a more extended Q-range, we interpreted[13] this increase in intensity to be due to scattering from crystals being formed, but the lower Q-limit of the scattering curves was too high to make a definite distinction between the two interpretations. However, using USAXS we see (Figure 5B) that the increasing scattered intensity at Q-values lower than 0.3 nm^{-1} is due to the scattering from crystals, showing a Porod slope of −4 in the log I vs log Q plot. Some oscillations are also observed which are due to the form factor of the crystals. We therefore believe that no second aggregation step of the colloidal aggregates occurs.

For the synthesis with Si/OH = 3.02 there appears to be a correlation between the intensity of the feature due to the scattering from the colloidal aggregates and the degree of crystallinity as determined from the WAXS-data (see Figure 7). At higher alkalinity (Si/OH = 2.42) we do not observe the presence of colloidal aggregates at any stage during the reaction. This suggests that the size of the particles consumed in the crystallization process is smaller than the minimum size probed by the SAXS and that the colloidal aggregates are just a kind of storage of amorphous silica in this oversaturated system.

Crystal Growth. Comparison of the growth rate of Si-TPA-MFI we observed (∼1.2 nm/min) with those reported by Sano et al.[44] by in situ observation of growing crystals shows that our results are between the length and width growth rates as determined by extrapolation of their data. From our USAXS data it is not possible to discern between the length and width growth rates, and the electron microscopy images demonstrate that with the shape of our crystals it is hard to define a length and width (see Figure 11). When comparing growth rates, one has to keep in mind that these are strongly dependent on factors like the chemical composition of the synthesis mixture, the temperature, aging histories, and agitation or stirring. Therefore, even when taking into account the differences in reaction temperature by an Arrhenius relationship with an activation energy for crystal growth of 50 kJ/mol (approximate average of values reported in literature[44,14]), faster[45] as well as slower[15] growth rates can be found. In agreement with light scattering results of Persson et al.[15] we found the growth rate to be about the same for synthesis mixtures of varying alkalinity. Contrary to their results (for Si/OH ≥ 2.72), we found the final size of the crystals to increase with increasing alkalinity (see Figure 9A,B). Fegan & Lowe[46] found a decreasing final crystal size for increasing alkalinity, but at very high alkalinities (Si/OH ≤ 2) the final crystal size increased again. This is probably due to a lower amount of viable nuclei forming at very high alkalinities and also due to the absence of a heterogeneous gel phase or colloidal amorphous aggregates which could promote nucleation, as for synthesis mixtures with Si/OH = 2.42.

From the USAXS results we see that the average size of the growing crystals is approximately the same for reaction times up to 150 min. The degree of crystallinity as determined from the WAXS results, being a measure for the volume of crystals in the sample, shows in the same time scale lower crystallinities for the sample with Si/OH = 2.42 compared to Si/OH = 3.02 (see Figure 7). These results agree with the presence of a lower number density of crystals in the case of the synthesis with the highest alkalinity.

The electron microscopy pictures confirmed the trend in the average particle size at various crystallization times and also showed that the population of crystals during and after the growth process is not monodisperse. Schoeman[47] recently found similar results using cryogenic-TEM, and his pictures also showed crystals which are irregularly shaped during the crystallization process.

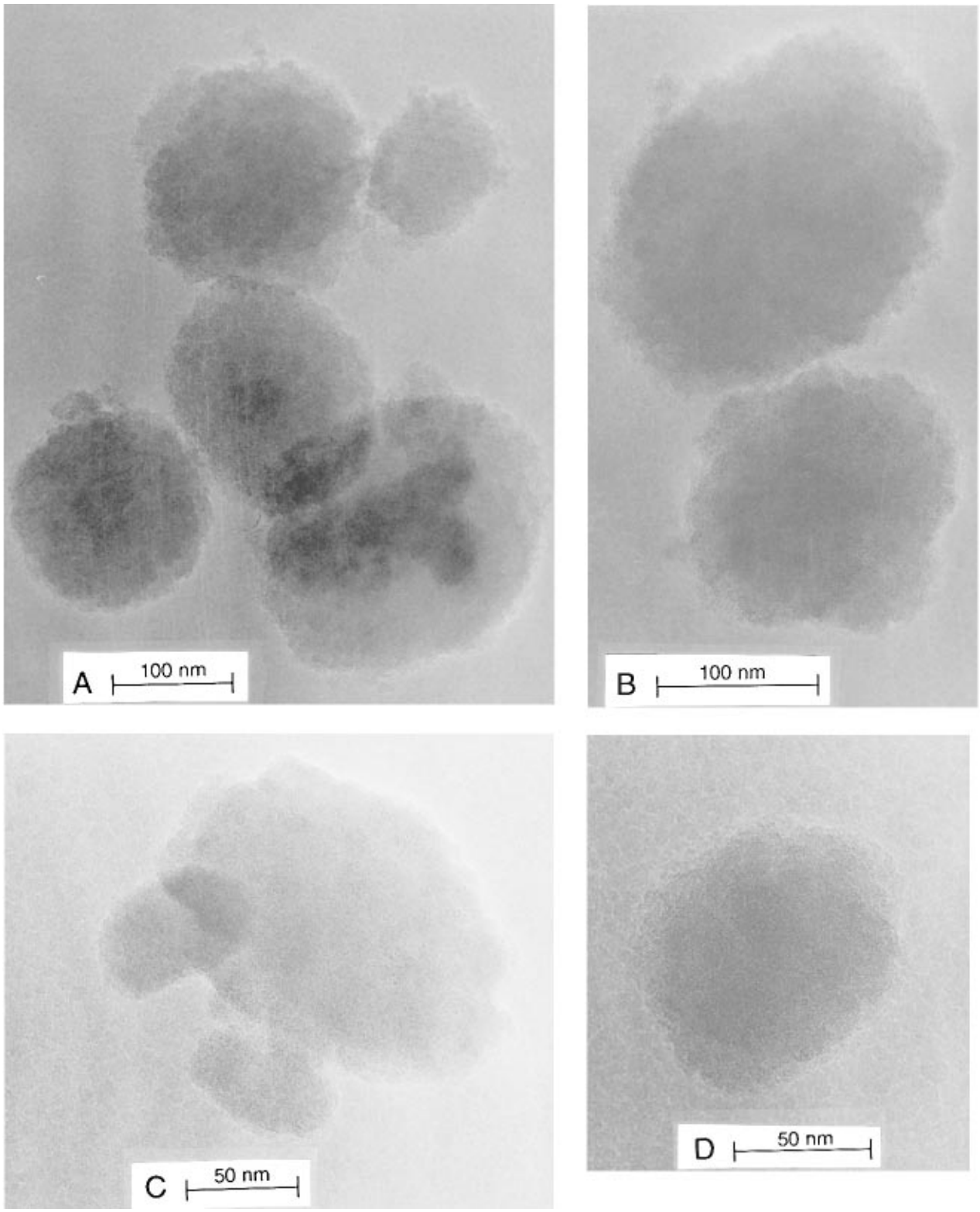

Figure 11. EM photographs of crystals: Si/OH = 2.42, t = 180 min (A) and (B); Si/OH = 3.02, t = 180 min (C) and (D).

Crystal Aggregation. At reaction times when the linear growth of the crystals has more or less finished (see Figure 9A,B), we found a sudden increase in scattering intensity in the low Q-range of the USAXS pattern (see Figure 10) for both synthesis mixture compositions. The slope of the straight fit in the log I vs log Q plot agrees with the scattering from mass fractal aggregates which are formed according to a diffusion-limited cluster aggregation process (DLCA).[21,27] The size of the aggregates can be determined by the transition where the linear fit levels off with decreasing angle. However, the lowest Q-angle probed by the USAXS is still too large to be able to determine the size of the aggregates, so they must be larger than 6 μm. This points to a sudden aggregation of the crystals, for Si/OH = 2.42 to occur between a reaction time of 286 and 312 min, and for Si/OH = 3.02 between 183 and 220 min (no patterns are available between these times). Figure 9 shows that this aggregation step occurs when the linear growth of the crystals had finished. This sudden aggregation process could be related to a change in the composition of the solution. Fegan and Lowe[46] pointed out that there can be a sudden change in silicate ion concentration in the solution when the crystallization is in such an advanced stage that all polymeric amorphous silica

is consumed. The crystalline phase then controls the silicate ion concentration, and since the solubility of the crystalline phase is far lower than that of the amorphous phase, the silicate ion concentration markedly decreases. For Si/OH-values higher than or equal to 2.0, this effect is accompanied by an increase in the pH. These changes solution composition might effect the repulsive forces between the individual crystals such that upon a collision of the crystals a high probability of coagulation exists. In this case the aggregation of the crystals will show a crossover from the (slow) reaction-limited type to the fast diffusion-limited type and may result in aggregates having mass fractal properties with a fractal dimension of about −1.8. In the electron microscopy pictures these aggregates were not found (Figure 11), which is not surprising taking into account the invasive nature of the sample treatment for electron microscopy and the vulnerability of the aggregates formed according to a diffusion-limited cluster aggregation process.

Conclusions

Our simultaneous SAXS and WAXS results showed that crystallization of Si-TPA-MFI is possible directly from a clear solution without the presence of an amorphous gel phase during any stage of the crystallization process for a synthesis mixture with Si/OH = 2.42. Colloidal amorphous aggregates were formed in the solution prior to the onset of crystallization for a solution with Si/OH = 3.02. The USAXS results pointed out that these particles did not show a secondary aggregation step[11] but are most likely to be a source of nutrients which will dissolve to subcolloidal particles and/or silicate ions which are consumed in the crystallization process.

Our in situ USAXS experiments also showed that the MFI crystals grow linearly with time and that the growth rate is the same for both alkalinities studied. The final crystal size however was larger for the higher alkalinity which can be explained in terms of less viable nuclei being formed, resulting in a lower concentration of crystals. Fitting of the USAXS patterns showed that the crystal population was rather polydisperse during the growth stage, which was confirmed by electron micrographs. These micrographs also showed that the growing crystals do not exhibit nice crystal faces but are more or less spherical with a relatively rough surface.

With the extended *Q*-range available with the USAXS method we were able to monitor in situ the aggregation process of the discrete crystals when the crystal growth approaches completion, which is probably related with the sudden changes in the composition of the liquid phase in this stage.

Acknowledgment. We acknowledge W. van Herpen for the development and construction of the rotating heated cell. Dr. P. J. Kooyman of the National Centre for High Resolution Electron Microscopy, Delft University of Technology, Delft, The Netherlands, is acknowledged for performing the electron microscopy investigations. We thank Dr. E. Pantos for stimulating discussions. SAXS/WAXS experiments were performed at the Daresbury Synchrotron Radiation Source by an EPSRC grant. USAXS experiments were performed at the European Synchrotron Radiation Facility under Grants SC-138 and SC-202.

References and Notes

(1) Van Bekkum, H., Flanigen, E. M., Jansen, J. C. (Eds. *Introduction to zeolite science and practice*; Studies in surface science and catalysis; Elsevier: Amsterdam, 1991; Vol. 58.

(2) Fan, W.; Li, R.; Ma, J.; Fan, B.; Dou, T.; Cao, J. *Micropor. Mater.* **1997**, *8*, 131−140.

(3) R. M. Barrer, *Hydrothermal Chemistry of Zeolites*; Academic Press: London, 1982.

(4) Davis, M. E.; Lobo, R. F. *Chem. Mater.* **1992**, *4*, 756−768.

(5) Burkett, S. L.; Davis, M. E. *Chem. Mater.* **1995**, *7*, 920−928.

(6) Burkett, S. L.; Davis, M. E. *Chem. Mater.* **1995**, *7*, 1453−1463.

(7) Lobo, R. F.; Zones, S. I.; Davis, M. E. *J. Inclusion Phenom. Mol. Recognit. Chem.* **1995**, *21*, 47−78.

(8) Burkett, S. L.; Davis, M. E. *J. Phys. Chem.* **1994**, *98*, 4647−4653.

(9) Helmkamp, M. M.; Davis, M. E. *Annu. Rev. Mater. Sci.* **1995**, *25*, 161−192.

(10) Kubota, Y.; Helmkamp, M. M.; Zones, S. I.; Davis, M. E. *Micropor. Mater.* **1996**, *6*, 213−229.

(11) Dokter, W. H.; Van Garderen, H. F.; Beelen, T. P. M.; Van Santen, R. A.; Bras, W. *Angew. Chem., Int. Ed. Engl.* **1995**, *34*, 73−75.

(12) Jullien, R.; Botet, R. *Aggregation and fractal aggregates*; World Scientific: Singapore, 1987.

(13) De Moor, P.-P. E. A.; Beelen, T. P. M.; Van Santen, R. A. *Micropor. Mater.* **1997**, *9*, 117−130.

(14) Schoeman, B. J.; Sterte, J.; Otterstedt, J. E. *Zeolites* **1994**, *14*, 568−575.

(15) Persson, A. E.; Schoeman, B. J.; Sterte, J.; Otterstedt, J. E. *Zeolites* **1994**, *14*, 557−567.

(16) Diat, O.; Bösecke, P.; Ferrero, C.; Freund, A. K.; Lambard, J.; Heintzmann, R. *Nucl. Instrum. Methods Phys. Res. Sect. A* **1995**, *356*, 566−572.

(17) Diat, O.; Bösecke, P.; Lambard, J.; de Moor, P.-P. E. A. *J. Appl. Cryst.*, in press.

(18) Bösecke, P. *Rev. Sci. Instrum.* **1992**, *63*, 438−441.

(19) Bösecke, P.; Diat, O.; Rasmussen, B. *Rev. Sci. Instrum.* **1995**, *66*, 1636−1638.

(20) Glatter, O.; Kratky, O. *Small Angle X-Ray Scattering*; Academic Press: New York, 1982.

(21) Teixeira, J. in: Stanley, H. E.; Ostrowsky, N. *On Growth and Form: Fractal and non-fractal Patterns in Physics*; NATO-ASI Series E100; Martinus Nijhoff Publishers: Dordrecht, 1986; pp 145−162.

(22) Guinier, A.; Fournet, G. *Small Angle Scattering of X-Rays*; Wiley: New York; Chapman Hall: London, 1955.

(23) Pedersen, J. S. *Adv. Colloid Interface Sci.* **1997**, *70*, 171−210.

(24) Mulato, M.; Chambouleyron, I. *J. Appl. Cryst.* **1996**, *29*, 29−36.

(25) Porod, G. *Monatsh. Chem.* **1972**, *103*, 395−405.

(26) Schmidt, P. W. In *The fractal approach to heterogeneous chemistry*; Avnir, D., Ed.; John Wiley & Sons Ltd.: New York, 1989; pp 67−79.

(27) Meakin, P. In *On growth and form*; NATO ASI Ser. E100; Martinus Nijhof: Dordrecht, 1986; pp 111−135.

(28) Olivi-Tran, N.; Thouy, R.; Jullien, R. *J. Phys. I France* **1996**, *6*, 557−574.

(29) Bale, H. D.; Schmidt, P. W. *Phys. Rev. Lett.* **1984**, *53*, 596−599.

(30) Schmidt, P. W. *J. Appl. Cryst.* **1991**, *24*, 414−435.

(31) Reference 20, pp 119−125.

(32) Reference 22, pp 111−120.

(33) Schmidt, P. W. *J. Appl. Cryst*, **1988**, *21*, 602−612.

(34) Lambard, J.; Lesieur, P.; Zemb, T. *J. Phys. 1 France* **1992**, *2*, 1191−1213.

(35) Lake, J. A. *Acta Crystallogr.* **1967**, *23*, 191−194.

(36) Verduijn, J. P. Exxon patent, PCT/EP92/02386.

(37) Bras, W.; Derbyshire, G. E.; Ryan, A. J.; Mant, G. R.; Felton, A.; Lewis, R. A.; Hall, C. J.; Greaves, G. N. *Nucl. Instrum. Methods Phys. Res. Sect. A* **1993,** *326*, 587−591.

(38) Lewis, R. A.; Fore, N. S.; Helsby, W.; Hall, C.; Jones, A.; Parker, B.; Sumner, I.; Worgan, J. S.; Budtz-Jorgensen, C. *Rev. Sci. Instrum.* **1992**, *63*, 642−647.

(39) Höhr, A.; Neumann, H. B.; Schmidt, P. W.; Pfeifer, P.; Avnir, D. *Phys. Rev. B* **1988**, *38*, 1462−1467.

(40) Reference 20, pp 38−41; 189−191.

(41) Cundy, C. S.; Henty, M. S.; Plaisted, R. J. *Zeolites* **1995**, *15*, 342−352.

(42) Hay D. G.; Jaeger, H.; Wishier, K. G. *Zeolites* **1990**, *10*, 571−576.

(43) Jansen, J. C. In *Introduction to zeolite science and practice*; Van Bekkum, H., Flanigen, E. M., Jansen, J. C., Eds.; Studies in surface science and catalysis; Elsevier: Amsterdam, 1991; Vol. 58, pp 77−130.

(44) Sano, T.; Sugawara, S.; Kawakami, Y.; Iwasaki, A.; Hirata, M.; Kudo, I.; Ito, M.; Watanabe, M. In *Zeolites and Related Microporous Materials: State of the Art 1994*; Studies in Surface Science and Catalysis; Elsevier Science: Amsterdam, 1994; Vol. 84.

(45) Cundy, C. S.; Lowe, B. M.; Sinclair, D. M. *J. Cryst. Growth* **1990**, *100*, 189−202.

(46) Fegan, S. G.; Lowe, B. M. *J. Chem. Soc., Faraday Trans. 1* **1986**, *82*, 785−799.

(47) Schoeman, B. J. *Zeolites* **1997**, *18*, 97−105.